scientific reports

Check for updates

OPEN

LncRNA NEAT1 regulation of the miR-101-3p/RAC1 axis affects cervical cancer aerobic glycolysis and progression

Lingling Cao[1,4], Wumidan Abudureheman[1,4], Guqun Shen[2], Yunshan Ouyang[1], Wang Yang[1], Qian Zhao[1], Tianze Lu[3] & Chen Lin[1]✉

Cervical cancer is a prevalent malignancy among women worldwide. Long-chain non-coding rna (lncRNAs) play a key role in the development of several cancers. Here, we found that the expression of lncRNA NEAT1 was significantly increased in cervical cancer cells and tissues and was closely associated with poor patient prognosis. Subsequently, we found that down-regulation of NEAT1 inhibited the proliferation, migration and invasion of cervical cancer cells. Subsequent studies showed that NEAT1, a competitive endogenous RNA, effectively enhanced RAC1 expression by adsorbing miR-101-3p. Glycolysis-related genes were predicted to be enriched in cervical cancers with high NEAT1 expression by bioinformatics analysis and confirmed by in vivo experiments. Our results suggest that NEAT1 enhances the Warburg effect through the miR-101-3p/RAC1 axis and promotes the proliferation, migration and invasion of cervical cancer cells. Therefore, elucidating this potential mechanism and targeting the NEAT1/miR-101-3p/RAC1 pathway may provide valuable insights.

Keywords LncRNA NEAT1, Cervical cancer, miR-101-3p, RAC1, Glycolysis

Cervical cancer (CC) continues to be a prevalent and serious health issue for women globally, with an increasing incidence noted among younger women[1]. While advancements have been made in diagnosing and treating CC, outcomes for patients with advanced or recurrent forms of the disease remain unfavorable[2]. Thus, a deeper understanding of the biology of CC cells is crucial for developing new therapeutic strategies to enhance patient survival rates.

Long non-coding RNAs (lncRNAs), which are transcripts longer than 200 nucleotides without protein-coding potential[3–6], have increasingly been linked to cancer development, progression, and outcomes[7]. Yuan et al. reported differential expression of 190 lncRNAs and 2326 protein-coding genes in cervical cancerpatient samples[8]. Another study identified 5844 lncRNAs and 4436 genes that were aberrantly expressed in CC compared to normal cervical tissue[9]. NEAT1, a recently identified lncRNA[10], has been shown to facilitate the progression of various cancers, including breast and lung cancer[11,12]. Shen et al. observed that NEAT1 was overexpressed in CC, potentially enhancing migration and invasion by regulating the miR-124/NF-κB axis[13]. Furthermore, NEAT1 has been implicated in promoting CC cell growth by sponging the miR-664b-3p/Rheb/mTOR pathway[14], yet the precise mechanisms of NEAT1 in CC remain poorly understood.

Metabolic reprogramming from oxidative phosphorylation to aerobic glycolysis, known as the "Warburg effect" is a cancer hallmark, crucial for rapid cancer growth, survival, and invasion[15]. lncRNAs are known to regulate glucose metabolism by influencing metabolic enzyme and transporter expression or by altering signaling pathways. Key enzymes such as hexokinase-2 (HK-2), pyruvate kinase M2 (PKM2), glucose transporter protein-1 (GLUT-1), and lactate dehydrogenase-1 (LDH-1) are integral in regulating the Warburg effect[16]. Zhang et al. found that mTORC1 inhibited NEAT1_2 expression and NEAT1_2-dependent paranuclear speckled biogenesis, thereby promoting mRNA splicing and expression of key glycolytic enzymes, enhancing the Warburg effect in hepatocellular carcinoma[17]. The classical metabolic regulator, c-Myc, mediates glucose metabolism reprogramming by targeting glycolytic enzymes[18]. NEAT1's role in tumorigenesis has been

[1]Xinjiang Key Laboratory of Molecular Biology of Endemic Diseases, School of Basic Medical Science, Xinjiang Medical University, Xinjiang Medical University Graduate School, Urumqi 830017, Xinjiang, China. [2]Department of Gynecological Surgery, The Third Affiliated Cancer Hospital of Xinjiang Medical University, Urumqi 830011, Xinjiang, China. [3]Xinjiang Medical University Tumor Hospital, Urumqi 830011, Xinjiang, China. [4]Lingling Cao and Wumidan Abudureheman have contributed equally to this work. ✉email: linmao1977@126.com

demonstrated through various transfection, carcinogen studies, and expression analyses[19–21]. However, the role of NEAT1 in enhancing glucose metabolism during CC progression remains unclear.

This study found that NEAT1 expression was upregulated in CC tissues and cells, correlating with poor prognosis. We explored the regulatory mechanism of NEAT1 silencing in CC and demonstrated that NEAT1 acts as a competitive endogenous RNA, enhancing RAC1 expression by sponging miR-101-3p. Comprehensive bioinformatics analysis showed that glycolysis-related genes were prevalent in CC with high NEAT1 expression. In vivo experiments confirmed that silencing NEAT1 inhibited aerobic glycolysis and CC progression, suggesting that the NEAT1/miR-101-3p/RAC1 axis could be a novel target for CC treatment.

Materials and methods

Cell culture and cell transfection

C33A, HeLa, SiHa, and H8 cell lines come from Shanghai Hongsheng Biotechnology Co., Ltd. Cells were under suitable conditions to culture. The cells were transfected with a lentiviral vector (shNEAT1) from Shanghai Jikai Genetics Co., following the provided instructions. Transfection efficiency, indicated by GFP fluorescence, was evaluated using inverted fluorescence microscopy (TI-DH611624, Nikon, Japan), and NEAT1 knockdown was confirmed via qRT-PCR. The study's control group included HeLa and SiHa cells transduced with empty lentiviral vectors, while the experimental group comprised cells transduced with shNEAT1-containing vectors, designated as shNC-HeLa, shNEAT1-HeLa, shNC-SiHa, and shNEAT1-SiHa. The NEAT1 knockdown vector, GV493, was constructed with the sequence: hu6-MCS-cBh-GFP-IRES-puro.

Patients and clinical specimens

Thirty cervical cancer patients and thirty patients undergoing total uterine resection for conditions such as uterine fibroids or polyps were enrolled in this study from April 2023 to October 2023 at the Third Affiliated Cancer Hospital of Xinjiang Medical University. None of the patients received preoperative radiotherapy, chemotherapy, or targeted therapy. All were diagnosed with cervical cancer via postoperative pathology.

qRT-PCR

RNA extraction was performed using the TRIzol kit (ER501-01-V2, Allotype Gold) according to the manufacturer's instructions. Reverse transcription was performed using the PrimeScriptTM RT kit (RR047A, Takara). Subsequently, the synthesized complementary DNA (cDNA) was amplified using SYBR premixed Ex Taq II kit (RR820A, Takara). The relative abundance of RNA gene expression was calculated using the $2^{-\Delta\Delta Ct}$ method. The primer sequences were as Table 1.

EdU assay

An EdU proliferation assay was employed to assess cell proliferation. Ten micromolar EdU (C0075S, BeoTemi Biotech) was introduced to the cells 48 h post-infection. EdU-positive cells were visualized through fluorescence microscopy.

Scratch wound healing assay and transwell invasion and migration assays

In the wound healing assay, cells were seeded into six-well plates and incubated overnight. Wounds were formed by scraping a monolayer of cells with a pipette tip and washing them with culture medium. The cells were then incubated in medium-containing culture solution for 24 h and photographs were taken for documentation. Transwell migration experiment: The Transwell chamber was placed in a 24-well plate, and the upper chamber was pre-incubated with serum-free medium for 30 min. The cell density was adjusted to 1×10^5 cells/mL by re-suspension in serum-free medium. 200 µL cell suspension was added to the upper chamber, and 500 µL complete medium containing 10% FBS was added to the lower chamber. Incubate at 37 ℃, 5% CO_2 incubator for 24 h. The non-migrating cells in the upper chamber were gently removed with a cotton swab, fixed with 4% paraformaldehyde for 30 min, and stained with 0.1% crystal violet for 20 min. The cells on the surface of the lower compartment membrane were observed and counted under a microscope. Transwell invasion experiment: Matrigel was diluted with serum-free medium at 1:8, 100 µL was evenly spread on Transwell cell membrane,

Genes	Forwards (5′-3′)	Reverse (5′-3′)
beta-Actin	CTGAACCAAGGAGACGGAATACA	GAAGGGCCGGTTCATGTCAT
GAPDH	GATTCCACCCATGGCAAATTC	CTGGAAGATGGTGATGGGATT
U6	CTCGCTTCGGCAGCACA	AACGCTTCACGAATTTGCGT
HK2	TCTACCACATGCGTCTCTCAGAT	ACCATTGTCTGTCACCCTTACTC
LDHA	AGCCTTGAACTCACTGTGTATCC	CATCCTGAGCCTGCATAGTCATA
GLUT1	GAATCGTCGTTGGCATCCTTATT	TCGTTACGATTGATGAGCAGGAA
PFKP	ATGCTATCTGAGGCTCGAAACAA	GTCCCACTGGCTGACTGTTTAAT
PKM2	TTGTACCATGCAGAGACCATCAA	AGGATGTTCTCGTCACACTTCTC
RAC1	AAATGTCCGTGCAAAGTGGTATC	AGCTTCTCAATGGTGTCCTTATCA
Homo-NEAT1	TGCCACAACGCAGATTGATG	ACAAGAAGGCAGGCAAACAG
hsa-miR-101-3p	TACAGTACTGTGATAACTGAA	–

Table 1. Sequences of primers of qPCR.

and incubated at 37℃ for 4–6 h until the matrix gel solidified. The cell density was adjusted to 5×10^4 cells/mL by re-suspension in serum-free medium. 200 μL cell suspension was added to the upper chamber, and 500 μL complete medium containing 10% FBS was added to the lower chamber. Incubate at 37℃, 5% CO_2 incubator for 48 h. The non-invasive cells in the upper chamber were gently removed with a cotton swab, fixed with 4% paraformaldehyde for 30 min, and stained with 0.1% crystal violet for 20 min. The cells on the surface of the lower compartment membrane were observed and counted under a microscope.

Colony formation assay

Cells were cultured and then fixed using formaldehyde and stained to crystal violet, with each step lasting for a duration of 15 min. Images were captured after staining, and the colony count was determined using ImageJ software.

Dual-luciferase reporter gene assay

Prediction of the interaction between NEAT1 and miR-101-3p using Starbase. NEAT1-WT or NEAT1-MUT using Lipofectamine3000. The interaction between miR-101-3p and RAC1 was investigated by a similar method.

RNA immunoprecipitation (RIP) assay and miRNA pull-down assay

RIP assay employed the RIP detection kit (P0101, P0102) from GeneSeed Biotech. HeLa cells were transfected. Following 48 h incubation period, lysed utilizing RIP lysis buffer. The cell lysates were at 4 °C with AGO2 antibody and IgG antibody, both conjugated to magnetic beads. RNA associated with the antibody-bead complexes was extracted, and used qRT-PCR to quantify the expression. This assay utilized the IgG antibody as a negative control. In the pull-down assay, biotinylated probes were transfected into cell. Then harvested and processed in accordance with the instructions supplied with the miRNA pull-down kit (Bes5108, BersinBio). Cell lysates at 4 °C with streptavidin-coated magnetic beads in order to purify or enrich miRNA-RNA complexes. RNA extracted from the input sample served as a control, while the RNA associated with the beads was designated as the RPD group. The enriched RNA underwent elution, purification, and qRT-PCR analysis to evaluate specific RNA levels.

Western blotting

Proteins extracted from cells and quantified according to the instructions, then electrotransferred to a PVDF membrane and exposed after closed incubation and membrane washing. Antibody information is shown in Table 2.

Animal experiments

A total of 24 BALB/c female nude mice aged 4–5 weeks were selected and grouped by random number table method. The procedure is as follows: 24 nude mice are numbered from 1 to 24 by weight. Select an arbitrary starting point from the random number table and read random numbers in turn. The random numbers read are corresponding to the nude mouse number in order, and sorted according to the number size. The sorted nude mice were divided into 4 groups: shNC-HeLa group, shNEAT1-HeLa group, shNC-SiHa group and shNEAT1-SiHa group, with 6 mice in each group. The baseline characteristics such as body weight and age of nude mice in each group were compared to ensure that there were no significant differences between the groups, so as to ensure randomness and comparability of the experiment. To establish a cervical cancer lung metastasis model, each mouse was injected with 5×10^6 cells suspended in 200 μL PBS in the tail vein. In vivo bioluminescence imaging was performed using the IVIS Spectral Imaging System (PerkinElmer) on days 7, 14, and 21 post-injection to monitor tumor metastasis. The mice were euthanized at the end of the study (sodium pentobarbital anesthetic was made into a 1% solution in saline and injected intraperitoneally at a dose of 50 mg/kg) and their lungs and livers were collected for photographic documentation.

Metabolic measurements

Glucose uptake, lactate, and ATP assay kits were used. All assays followed the manufacturer's protocols.

Antibody	Dilution ratio	Manufacturer	Cat. no
HK2	1:1000	Cell signaling technology	2867T
PKM2	1:1000	Cell signaling technology	A21052
PFKP	1:1000	Cell signaling technology	A20983
RAC1	1:1000	Cell signaling technology	4651T
GLUT1	1: 5000	Proteintech	21829-1-AP
LDHA	1: 4000	Proteintech	19987-1-AP
β-actin	1: 5000	Affinity	AF7018
Goat Anti-Rabbit IgG H&L (HRP)	1: 5000	Affinity	S0011

Table 2. Antibody information.

H&E and IHC

Lung tissue samples were fixed in formalin and then embedded in paraffin blocks for sectioning. Histologic features were evaluated using H&E staining of the sections. Sections were exposed to for 10 min. Incubated overnight at 4℃ with RAC1 antibody (1:300, 24072-1-AP, Proteintech). Subsequently, secondary antibody, followed by a 30 min incubation with a streptavidin–biotin complex (Boster, USA). IHC staining was quantified using ImageJ software.

FISH

Tissues were fixed after cleaning. Tissues are sectioned, deparaffinized, repaired, and digested. Following a 1 h incubation at 40 °C, the prehybridization solution is replaced with a hybridization solution containing the miR-101-3p probe. Tissues were hybridized overnight at a constant temperature. The hybridization solution was subsequently washed away. Sections were stained with DAPI in an environment protected from light, rinsed and sealed with a fluorescence quenching sealer. The sequence of the miR-101-3p probe is provided below: Forward: 5′-GCATCAGCACTGTGATAACTGA-3′, Reverse: 5′-TTCAGTTATCACAGTACTGTA-3′.

Ethics approval

The human specimen study was conducted in accordance with the Declaration of Helsinki and was approved by the Ethics Committee of Xinjiang Medical University (Ethics Approval No. 20200326-16). The ethics and care of all animal experiments received approval from the Animal Care and Ethics Committees of First Affiliated Hospital of Xinjiang Medical University (Grant No: IACUC-KT-20230831-08) and the Institutional Animal Care and Use Committee of China. All methods were in accordance the relevant protocols, guidelines and regulations. All human experiment and animal studies adhered to the ARRIVE 2.0 requirements, which included study design, animal numbers, randomization, and statistical methods.

Statistical analysis

GraphPad Prism 6.0 was used for statistical data analysis. Student's t-test or one-way ANOVA was used for statistical analysis. Differences were statistically significant when the p-value was < 0.05.

Results

Upregulation of NEAT1 expression in cervical cancer tissues and cell

Initially, we examined the expression patterns of NEAT1 across various normal and cancerous tissues using the TCGA database, revealing that NEAT1 expression was elevated in nearly all cancer types, including cervical cancer (Fig. 1A). Subsequent analysis of TCGA data indicated that NEAT1 levels were higher in cervical cancer tissues than in normal cervical tissues across 308 samples (Fig. 1B). A one-way COX regression analysis, alongside a correlation study of NEAT1 expression and clinical outcomes, identified NEAT1 as a risk factor for cervical cancer, with high NEAT1 expression associated with poorer prognosis in patients (n = 294, $p < 0.005$) (Fig. 1C,D). These findings suggest that NEAT1 may function as an oncogene in cervical cancer.

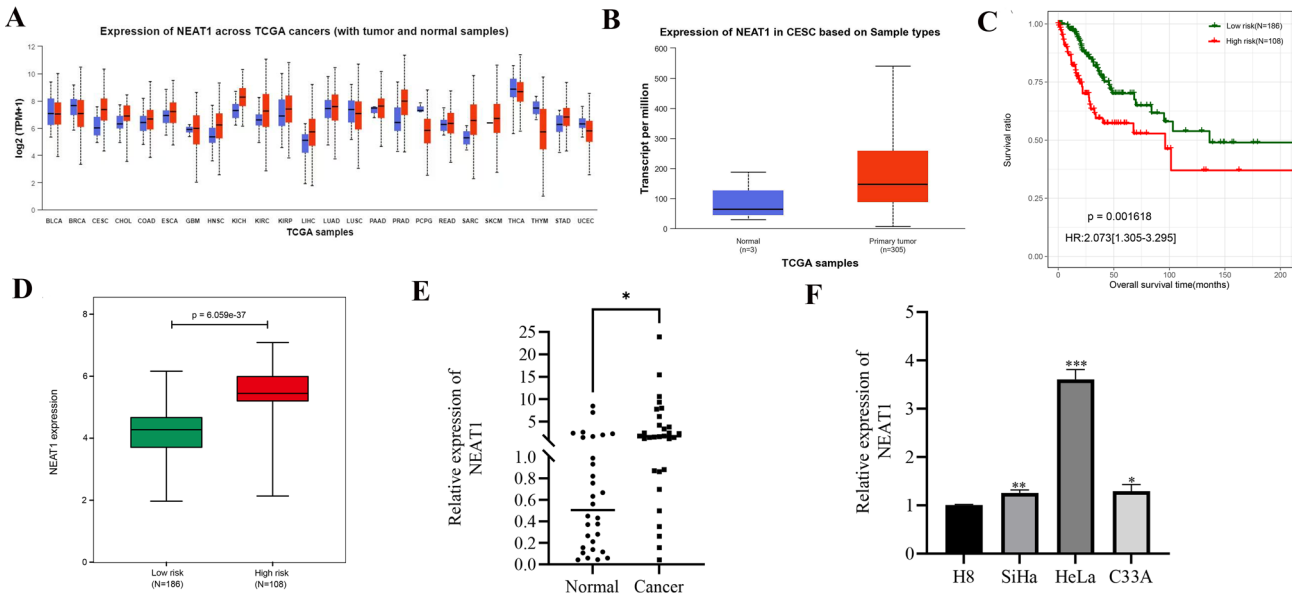

Fig. 1. NEAT1 is upregulated in human CC tissues and cells. (**A**) NEAT1 is expressed differently in various tumors. (**B**) Expression of NEAT1 in cervical squamous cell carcinoma from the UALCAN database. (**C**, **D**) Correlation between NEAT1 expression and clinical outcomes was examined through univariate COX regression analysis and NEAT1 expression. (**E**) Detection of NEAT1 expression levels in CC tissues (n = 30). (**F**) Levels of NEAT1 in different cervical cancer cells (SiHa, HeLa, C33A) and normal human cervical epithelial cell (H8). *$p < 0.05$; **$p < 0.01$; ***$p < 0.001$.

In addition, the expression of NEAT1 in CC tissues and cell lines was quantified by qRT-PCR, which showed that NEAT1 expression was upregulated in CC tissues and cells (Fig. 1E,F). The samples were then categorized into NEAT1 high-expression group (median = 14 or more) and low-expression group (median = 16 or less), and the correlation between NEAT1 levels and clinicopathological features including lymph node metastasis was detected using Fisher's exact test (Table 3).

Down-regulation of NEAT1 inhibits proliferation, migration and invasion of cervical cancer cells

In a subsequent study, HeLa and SiHa cervical cancer cells were transfected with lentiviral vectors either containing NEAT1 silencing constructs or empty vectors as controls. The control groups comprised HeLa and SiHa cells transduced with empty lentivirus, while the experimental groups included HeLa and SiHa cells transduced with lentiviral vectors designed to silence NEAT1, labeled as shNC-HeLa, shNEAT1-HeLa, shNC-SiHa, and shNEAT1-SiHa. The knockdown efficiency of NEAT1 was confirmed by qRT-PCR (Figs. 2A and S1), which demonstrated reduced NEAT1 expression in the experimental group compared to the control, confirming successful NEAT1 silencing in HeLa and SiHa cells.

The plate cloning and EdU proliferation assays further revealed that reduced expression of NEAT1 significantly restrained the proliferation of cervical cancer cells (Fig. 2B,C). In addition, wound healing and Transwell assays showed that silencing NEAT1 reduced the migration and invasion ability of cervical cancer cells (Fig. 2D,E). Taken together, these results suggest that inhibition of NEAT1 expression can effectively block the progression of CC cells.

NEAT1 functions as a sponge for miR-101-3p

The potential interaction site between NEAT1 and miR-101-3p was predicted using the Starbase tool (Fig. 3A). Fragments of wild-type NEAT1 (NEAT1-WT) and mutant NEAT1 (NEAT1-MUT) were engineered and inserted into the pmirGLO luciferase vector. Both NEAT1-WT/NEAT1-MUT and miR-101-3p mimic or miR-101-3p NC (negative control) mimic were co-transfected into HeLa cells using Lipofectamine 3000. Forty-eight hours post-transfection, luciferase activity was measured using a dual-luciferase reporter assay kit, revealing a notable decrease in reporter activity in the presence of miR-101-3p mimic (Fig. 3B). Further, qRT-PCR analysis showed that miR-101-3p levels were lower in cervical cancer cells compared to normal human cervical epithelial cells H8 (Fig. 3C). RIP assays were conducted to assess the association of NEAT1 and miR-101-3p with the AGO2 complex. The assays demonstrated significant enrichment of both NEAT1 and miR-101-3p in AGO2-containing complexes, compared to the IgG control, suggesting active participation in the RISC (Fig. 3D).

Characteristics	NEAT1 expression		*P*
	Low (n = 16)	High (n = 14)	
Age (years)	49.06 ± 12.36	50.93 ± 6.13	0.613
Tumor size (cm)			0.378
< 4	14 (87.50)	10 (71.43)	
≥ 4	2 (12.50)	4 (28.57)	
HPV			0.694
Positive	12 (75.00)	9 (64.29)	
Negative	4 (25.00)	5 (35.71)	
FIGO staging			0.675
I + II	13 (81.25)	10 (71.43)	
III + IV	3 (18.75)	4 (28.57)	
Cell differentiation			0.304
Poor	3 (18.75)	5 (35.71)	
Moderate	13 (81.25)	8 (57.14)	
Well	0 (0.00)	1 (7.14)	
Pathological type			1.000
Squamous carcinoma	13 (81.25)	12 (85.71)	
Adenocarcinoma	3 (18.75)	2 (14.29)	
Myometrial invasion			0.063
< 1/2	4 (25.00)	9 (64.29)	
≥ 1/2	12 (75.00)	5 (35.71)	
Lymph node metastasis			0.046*
Positive	14 (87.50)	7 (50.00)	
Negative	2 (12.50)	7 (50.00)	

Table 3. Relationship between lncRNA NEAT1 expression and clinical data of cervical cancer patients. *$P < 0.05$.

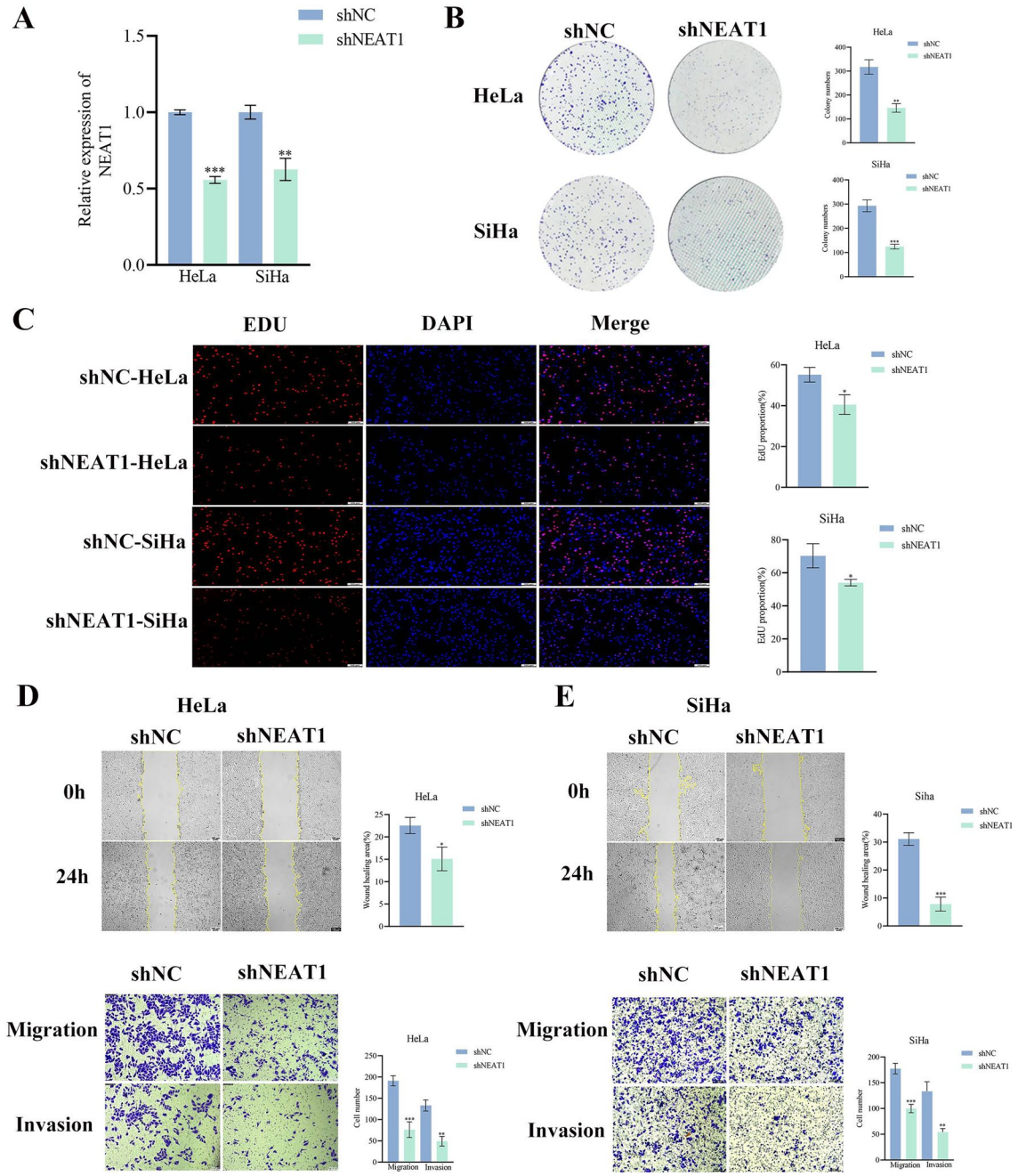

Fig. 2. The effect of NEAT1 on CC migration and invasion. (**A**) CC cells were transduced with lentiviral vectors to silence NEAT1, and silence efficiency was verified using qRT-PCR. (**B**, **C**) Plate cloning assay and EDU proliferation assay were performed to detect the effect of shNEAT1 on colony formation and proliferation of HeLa and SiHa cells. (**D**, **E**) Scratch wound healing assay and Transwell migration/invasion assay were used to detect the impact of shNEAT1 on the migration and invasion potential of HeLa and SiHa cells. $^{*}p < 0.05$; $^{**}p < 0.01$; $^{***}p < 0.001$.

In addition, RNA pull-down assay combined with qRT-PCR analysis showed significantly enhanced binding of NEAT1 to mir-101-3p specific probes compared to NC probes (Fig. 3E). These results collectively indicate that NEAT1 may act as a molecular sponge for miR-101-3p in CC, highlighting its role in post-transcriptional regulation by sequestering miR-101-3p and modulating its availability.

RAC1 is a Target of miR-101-3p

We identified binding sites for wild-type RAC1 (WT-RAC1) and mutant RAC1-type (MUT-RAC1) (Fig. 4A). co-transfection of WT-RAC1 with miR-101-3p mimics resulted in a significant decrease in reporter gene activity, indicating effective mirna-target interaction (Fig. 4B). In addition, qRT-PCR and IHC analyses showed elevated expression levels of RAC1 in cervical cancer cells and tissues (Fig. 4C,D).

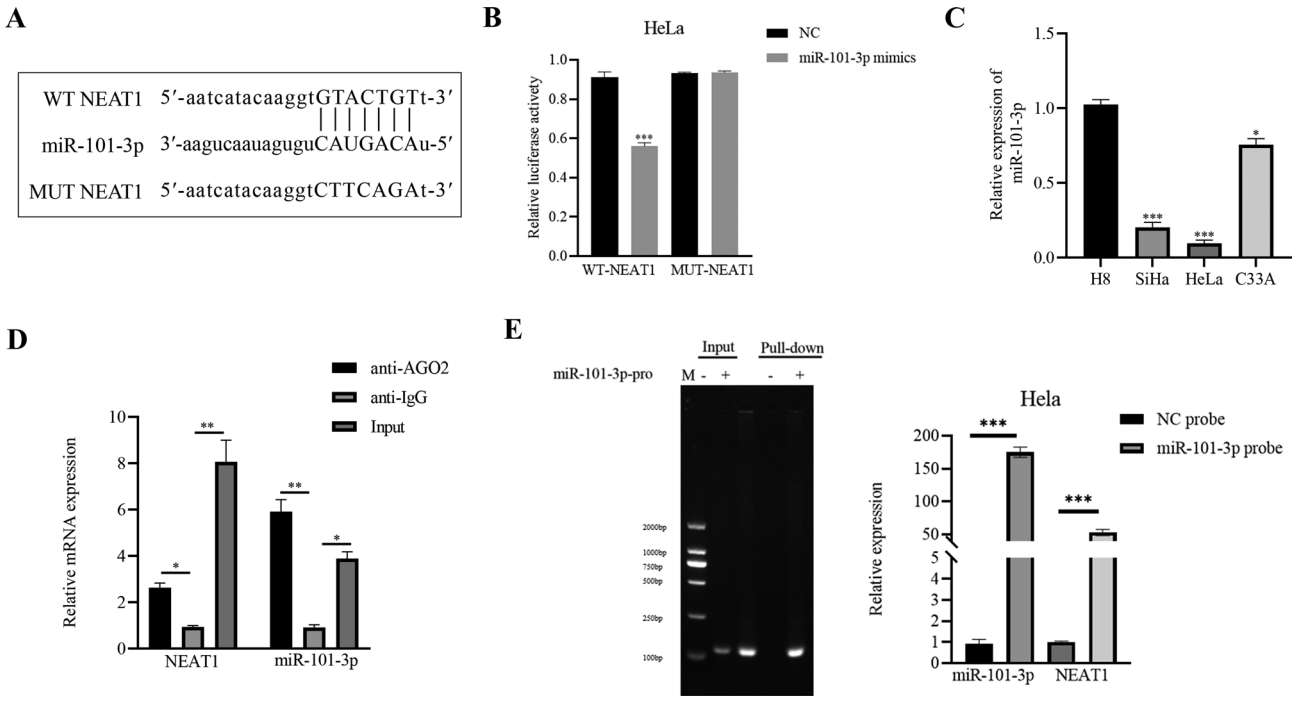

Fig. 3. miR-101-3p is an in vitro target of NEAT1. (**A**) Potential binding sites between NEAT1 and miR-101-3p were forecasted utilizing the Starbase platform. (**B**) For the dual-luciferase reporter gene assay, HeLa cells were co-transfected with either wild-type NEAT1 (WT-NEAT1) or mutated NEAT1 (MUT-NEAT1), along with miR-101-3p mimics or their corresponding negative controls. (**C**) The expression level of miR-101-3p in CC cells was assayed using qRT-PCR. (**D**) RIP assays demonstrated the interaction between NEAT1 and miR-101-3p. (**E**) RNA Pulldown experiments confirmed the direct interaction between miR-101-3p and NEAT1, with results presented as agarose gel electrophoresis showing NEAT1 amplification products at 154 bp.mRNA levels of miR-101-3p and NEAT1 were detected by qRT-PCR. All experiments were conducted in triplicate. Error bars represent mean ± standard deviation from at least three independent experiments. * $p < 0.05$; ** $p < 0.01$; *** $p < 0.001$.

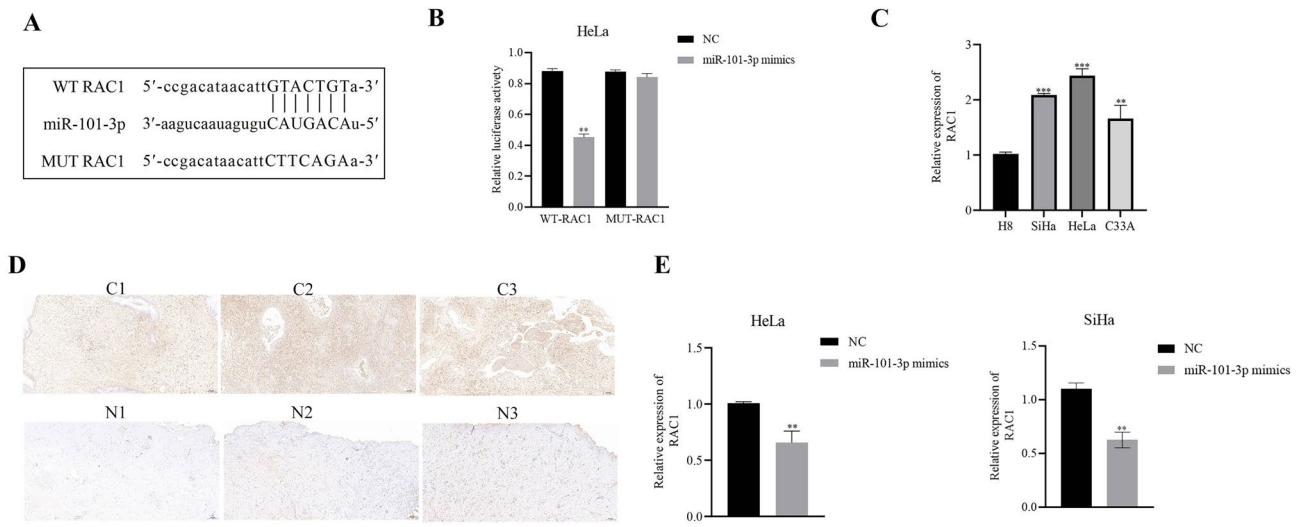

Fig. 4. miR-101-3p Targets RAC1. (**A**) Using Starbase, potential binding sites between RAC1 and miR-101-3p were predicted. (**B**) Conducting a dual luciferase reporter assay post-transfection. (**C**) qRT-PCR was performed to quantify RAC1 expression in CC cells. (**D**) Immunohistochemical detection of RAC1 expression in tissues (n = 3). (**E**) qRT-PCR analysis of RAC1 expression following transfection. ** $p < 0.01$; *** $p < 0.001$.

To further investigate the regulatory role of miR-101-3p on RAC1, we transfected HeLa cells with control miR-101-3p mimic or specific miR-101-3p mimic, respectively. After 48 h of transfection, the expression of RAC1 was detected by qRT-PCR. The results showed that RAC1 expression was reduced in cells transfected with miR-101-3p mimics (Fig. 4E), indicating that miR-101-3p negatively regulates RAC1 expression at the transcriptional level. Taken together, these findings support that RAC1 is a direct target of miR-101-3p in CC cells.

In vivo validation that knockdown of NEAT1 inhibits tumor metastasis

To explore whether NEAT1 influences cervical cancer progression via the miR-101-3p/RAC1 axis and the glycolytic pathway in vivo, we conducted a series of experiments. GFP-labeled HeLa and SiHa cells with silenced NEAT1 expression were generated using lentiviral vectors. Twenty-four BALB/c nude mice were randomly divided into four groups (n = 6 per group), and each mouse was intravenously injected with 5×10^6 cells in 200 µL via the tail vein to establish a lung metastasis model (Figs. 5A and S3). Tumor metastasis patterns were monitored every 7 days using the IVIS-PerkinElmer In Vivo Imaging System (BLI) (Fig. 5B), accompanied by quantitative BLI analysis. After three weeks, the mice were euthanized, and their lungs were examined for visually apparent tumor nodules on the surface (Fig. 5C). Lung tissue sections were also stained with H&E to assess the extent of tumor metastasis (Fig. 5D,E).

The results indicated that the NEAT1 knockdown group exhibited lower BLI fluorescence intensity compared to the control group, with significantly fewer and smaller tumor nodules. Conversely, H&E staining of lung tissues from control mice showed more extensive disruption of alveolar structures and visible metastatic tumor foci and necrotic cells. Ki-67 staining further confirmed that the proportion of positive cells (brown) in the shNEAT1 group was significantly reduced (Fig. 5F). Macroscopic tumor nodule counts, lung tissue H&E staining, and ki-67 were consistent with BLI data, suggesting that NEAT1 knockdown can slow the progression of CC metastasis in vivo.

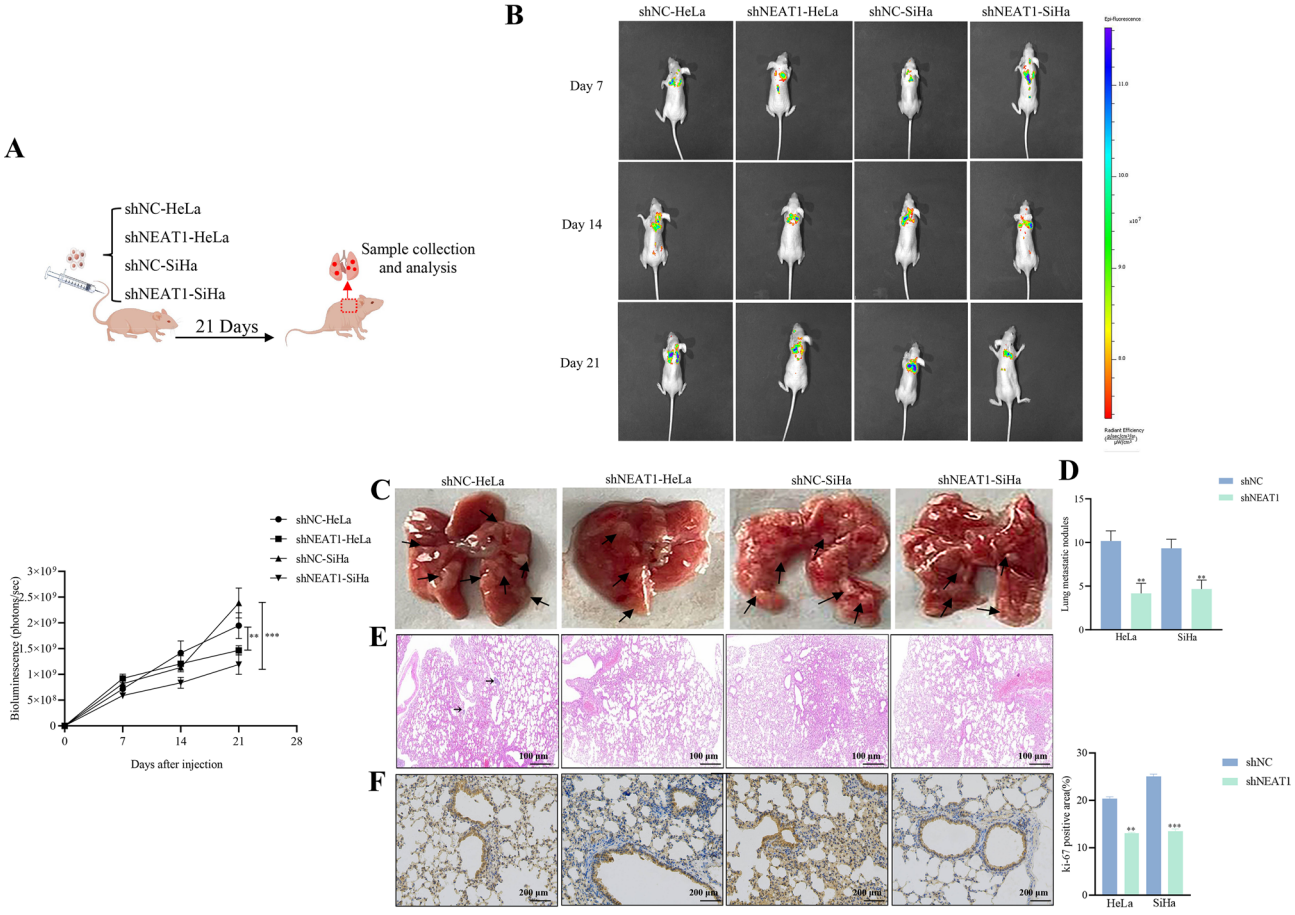

Fig. 5. In vivo validation that knockdown of NEAT1 inhibits tumor metastasis. (**A**) Experimental design: BALB/c nude mice underwent tail vein injection with shNC-SiHa, shNEAT1-SiHa, shNC-HeLa, or shNEAT1-HeLa cells, with a cohort of six animals per experimental group. (**B**) BLI took place on days 7, 14, and 21 after the injection, with intensity represented by color and fluorescence intensity. (**C**, **D**) Number of metastatic nodules isolated from nude mice injected via tail vein and (**E**) representative H&E-stained sections. Black arrows indicate metastatic nodules. (**F**) ki-67 was used to detect proliferation in each groupThree independent experiments were conducted. $^{**}p < 0.01$; $^{***}p < 0.001$.

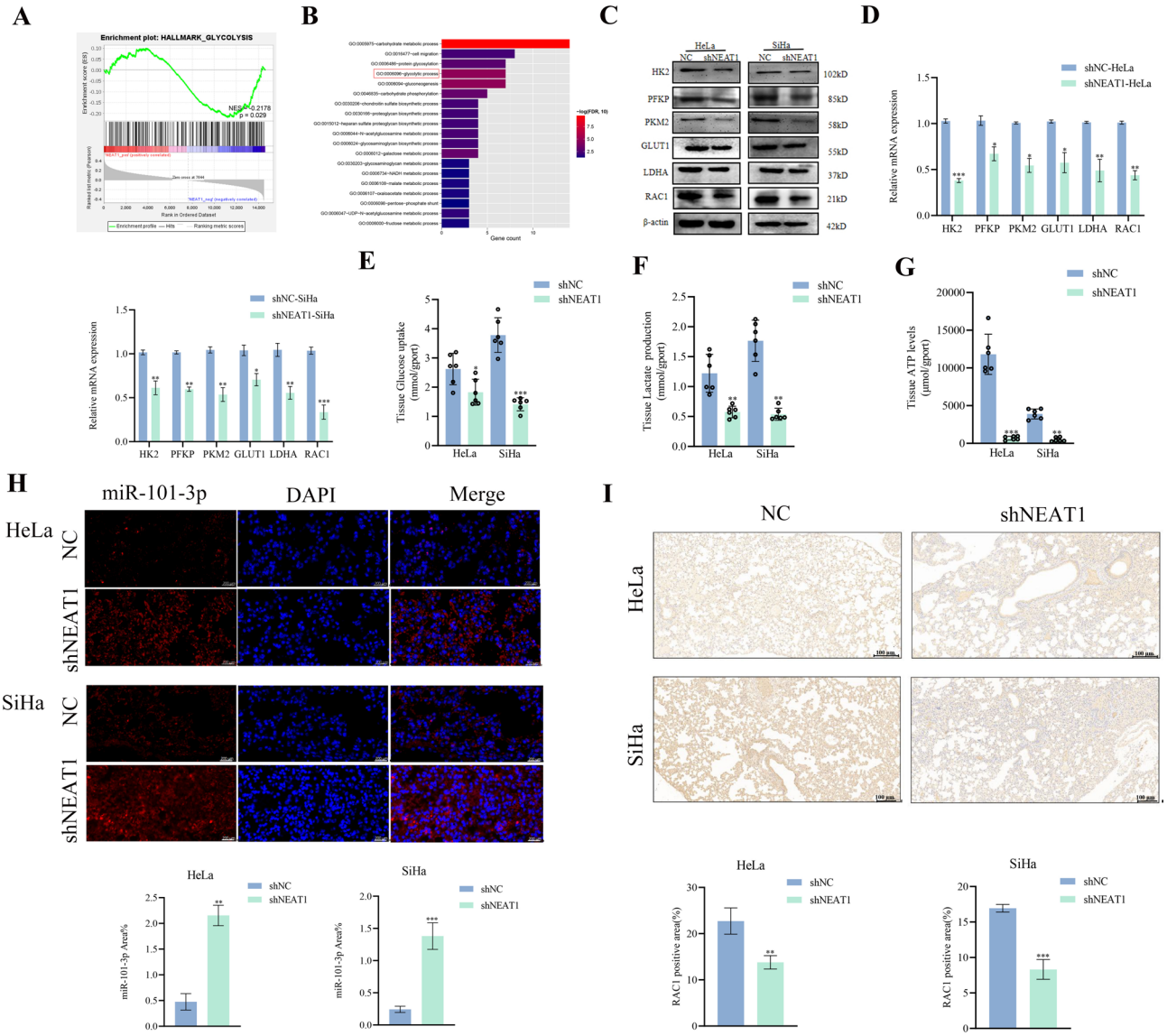

Fig. 6. LncRNA NEAT1 regulation of the miR-101-3p/RAC1 axis affects cervical cancer aerobic glycolysis and progression. (**A**) Correlation analysis plot between NEAT1 expression levels and the HALLMARK_GLYCOLYSIS pathway. (**B**) Graphical representation of GO functional annotations for genes within the HALLMARK_GLYCOLYSIS pathway significantly associated with NEAT1. (**C**) Western blotting and (**D**) qRT-PCR were employed to protein abundance and messenger RNA levels of genes associated with glycolysis, respectively, of glycolysis-related genes (HK2, PFKP, PKM2, GLUT1, LDHA) and the downstream target gene RAC1 in lung tissues (n = 3). (**E**, **F** and **G**) Quantification of glucose uptake, lactic acid production levels, and ATP generation in the lungs of nude mice were measured using relevant kits (n = 6). (**H**) FISH detection of miR-101-3p in nude mouse lungs (n = 3). (**I**) IHC examination of the downstream target gene RAC1(n = 3). $^{*}p < 0.05$; $^{**}p < 0.01$; $^{***}p < 0.001$.

LncRNA NEAT1 regulation of the miR-101-3p/RAC1 axis affects cervical cancer aerobic glycolysis and progression

Initially, we downloaded the Hallmark gene sets from the GSEA MSigDB database (https://www.gsea-msigdb.org/gsea/msigdb/index.jsp) and focused on the "HALLMARK_GLYCOLYSIS" pathway, which includes 200 relevant genes. Using the GSEA algorithm, we analyzed the correlation between lncRNA NEAT1 expression and the HALLMARK_GLYCOLYSIS pathway, revealing a significant negative correlation (Fig. 6A). Additionally, we utilized DAVID (https://david.ncifcrf.gov/) version 6.8 for GO functional enrichment analysis, setting an FDR threshold of < 0.05, and identified 19 significantly associated GO terms (Fig. 6B).

Western blot and qRT-PCR analyses were used to assess the levels of glycolysis-related proteins and transcripts in lung tissues, including HK2, PFKP, PKM2, GLUT1, LDHA, and the downstream target gene, RAC1. The results showed that the protein and transcript levels of these glycolysis-related genes were significantly reduced in the net1 knockout group (Figs. 6C,D and S4). This finding is consistent with our initial bioinformatics prediction.

Further analyses measuring glucose uptake, lactate production and ATP production in nude mouse lungs showed that the levels were all decreased in the NEAT1 down-regulated group (Fig. 6E,F,G). In addition, we examined the expression of miR-101-3p and its downstream target RAC1 using FISH and IHC (Fig. 6H,I) and found that miR-101-3p was up-regulated in the NEAT1 knockdown group while the corresponding RAC1 was down-regulated, emphasizing the NEAT1 effect on cervical cancer via the miR-101-3p/RAC1 axis progression through the miR-101-3p/RAC1 axis.

Discussion

Although the development of targeted therapies has provided new options for treating advanced and recurrent CC, the detailed mechanisms underlying CC progression and metastasis remain elusive[22]. Recent advances in the study of lncRNAs have shifted the perception of these molecules from mere "noise" in genomic transcription to crucial regulators of biological processes[23]. In our study, we found high expression of NEAT1 in CC tissues in public databases and collected clinical samples, and it was associated with poor patient prognosis and enhanced cell proliferation in vivo and in vitro. These findings define NEAT1 as an oncogene in CC.

Metabolic reprogramming to aerobic glycolysis offers cancer cells a growth advantage by providing energy for proliferation. lncRNAs have been identified as regulators of aerobic glycolysis in CC cells[24,25]. Recently, NEAT1 has been implicated in regulating glycolysis to accelerate tumor progression[26]. Specifically, NEAT1 has been shown to activate glycolysis, promoting proliferation and invasion in breast cancer[27] and to enhance glycolysis by stabilizing PGK1 in glioma progression[28]. Our comprehensive bioinformatics analysis showed that glycolysis-related genes were highly expressed in NEAT1-overexpressing CC, a finding that was also confirmed by in vivo experiments. Knockdown of NEAT1 resulted in reduced glucose uptake, lactate production, ATP production, and expression of glycolytic genes and proteins, thus demonstrating the role of NEAT1 in regulating glycolysis to accelerate tumor progression.

The ceRNA hypothesis introduces a novel regulatory mechanism where lncRNAs act as molecular sponges for specific miRNAs[29]. Emerging evidence supports NEAT1's role as a ceRNA[30]. Gao et al. reported that NEAT1 accelerates the development of thoracic aortic aneurysm by sponging miR-324-5p/RAN[31]. Wei et al. discovered that NEAT1 inhibits pancreatic cancer progression by targeting miR-146b-5p/traf6[32]. miR-101-3p has been been shown to be an oncogene in a variety of human malignant tumors[33,34]. Our research results revealed that the expression of miR-101-3p was decreased in CC cells. The potential sites for the binding of lncRNA NEAT1 to miR-101-3p were confirmed by the dual-luciferase reporter gene assay. It was also found through RIP-qPCR that in the immunoprecipitation complex of anti-AgO2 antibody, the enrichment degree of miR-101-3p by lncRNA NEAT1 was significantly higher than that of the IgG control group, confirming the co-localization of the two in RISC. In addition, The RNA Pulldown experiment further confirmed that the miR-101-3p probe transcribed in vitro could successfully capture NEAT1 at will, indicating a specific direct interaction between the two. These results jointly indicate that NEAT1, as a ceRNA, can sponge miR-101-3p. Ras-associated C3 botulinum toxin substrate 1 (RAC1) is a member of the Rho GTPase family, which plays an important role in the control of cellular motility, the regulation of oxidative stress, the surveillance of inflammation, and immunity, and has been regarded as a potential therapeutic target for cancer[35]. Ni et al[36] showed that RAC1 is highly expressed in lung cancer and promotes metastasis of lung cancer cells. Wang et al[37] verified RACl as an existing target of MEG3 by specific base pairing of its 3'-UTR in their study on thyroid cancer and resulted in transcriptional repression. In this study, RACl was found to be an important downstream target of miR-101-3p by Starbase database prediction and validation, and miR-101-3p was found to have a targeting relationship with RAC1. In addition, RAC1 was also found to be highly expressed in cervical cancer cells, and RAC1 expression was significantly decreased after overexpression of miR-101-3p, suggesting that miR-101-3p targets negatively regulate RAC1.

This study also has shortcomings, and to improve the clinical relevance of the findings, more diverse clinical samples should be collected to identify NEAT1 as a prognostic factor.

In conclusion, our results suggest that NEAT1, whose expression is increased in CC, enhances RAC1 expression by sponging miR-101-3p, thereby promoting CC progression through glucose metabolic reprogramming. These data suggest that all three may be potential molecular targets for the treatment of CC.

Data availability

Data is provided within the manuscript or supplementary information files.

Received: 19 December 2024; Accepted: 7 May 2025
Published online: 20 May 2025

References

1. Bray, F. et al. GLOBOCAN estimates of incidence and mortality worldwide for 36 cancers in 185 countries. *CA Cancer J. Clin.* **68**(2018), 394–424. https://doi.org/10.3322/caac.21492 (2018).
2. Arbyn, M. et al. Estimates of incidence and mortality of cervical cancer in 2018: A worldwide analysis. *Lancet Glob. Health* **8**, e191–e203. https://doi.org/10.1016/S2214-109X(19)30482-6 (2020).
3. Li, J. et al. LncRNA profile study reveals a three-lncRNA signature associated with the survival of patients with oesophageal squamous cell carcinoma. *Gut* **63**, 1700–1710. https://doi.org/10.1136/gutjnl-2013-305806 (2014).
4. Li, J. et al. LincK contributes to breast tumorigenesis by promoting proliferation and epithelial-to-mesenchymal transition. *J. Hematol. Oncol.* **12**, 19. https://doi.org/10.1186/s13045-019-0707-8 (2019).
5. Ni, W. et al. Long noncoding RNA GAS5 inhibits progression of colorectal cancer by interacting with and triggering YAP phosphorylation and degradation and is negatively regulated by the m6A reader YTHDF3. *Mol. Cancer* **18**, 143. https://doi.org/10.1186/s12943-019-1079-y (2019).
6. Alvarez-Dominguez, J. R. et al. Global discovery of erythroid long noncoding RNAs reveals novel regulators of red cell maturation. *Blood* **123**, 570–581. https://doi.org/10.1182/blood-2013-10-530683 (2014).

7. Xu, P. et al. The USP21/YY1/SNHG16 axis contributes to tumor proliferation, migration, and invasion of non-small-cell lung cancer. *Exp. Mol. Med.* **52**, 41–55. https://doi.org/10.1038/s12276-019-0356-6 (2020).
8. Yuan, L. et al. The transcriptome profiles and methylation status revealed the potential cancer-related lncRNAs in patients with cervical cancer. *J. Cell. Physiol.* **234**, 9756–9763. https://doi.org/10.1002/jcp.27661 (2019).
9. Huang, J. et al. Identification of lncRNAs by microarray analysis reveals the potential role of lncRNAs in cervical cancer pathogenesis. *Oncol. Lett.* https://doi.org/10.3892/ol.2018.8037 (2018).
10. Yu, X., Li, Z., Zheng, H., Chan, M. T. V. & Wu, W. K. K. NEAT 1: A novel cancer-related long non-coding RNA. *Cell Prolif.* **50**, e12329. https://doi.org/10.1111/cpr.12329 (2017).
11. Li, X. et al. LncRNA NEAT1 silenced miR-133b promotes migration and invasion of breast cancer cells. *IJMS* **20**, 3616. https://doi.org/10.3390/ijms20153616 (2019).
12. Sun, C. et al. Long non-coding RNA NEAT1 promotes non-small cell lung cancer progression through regulation of miR-377-3p-E2F3 pathway. *Oncotarget* **7**, 51784–51814. https://doi.org/10.18632/oncotarget.10108 (2016).
13. Shen, X., Zhao, W., Zhang, Y. & Liang, B. Long non-coding RNA-NEAT1 promotes cell migration and invasion via regulating miR-124/NF-κB pathway in cervical cancer. *OTT* **13**, 3265–3276. https://doi.org/10.2147/OTT.S220306 (2020).
14. Yu, X. et al. LncRNA-HOTAIRM1 promotes aerobic glycolysis and proliferation in osteosarcoma via the miR -664b-3p/Rheb/mTOR pathway. *Cancer Sci.* **114**, 3537–3552. https://doi.org/10.1111/cas.15881 (2023).
15. Koppenol, W. H., Bounds, P. L. & Dang, C. V. Otto Warburg's contributions to current concepts of cancer metabolism. *Nat. Rev. Cancer* **11**, 325–337. https://doi.org/10.1038/nrc3038 (2011).
16. Li, B. & Sui, L. Metabolic reprogramming in cervical cancer and metabolomics perspectives. *Nutr. Metab. (Lond.)* **18**, 93. https://doi.org/10.1186/s12986-021-00615-7 (2021).
17. Zhang, H., Su, X., Burley, S. K. & Zheng, X. F. S. mTOR regulates aerobic glycolysis through NEAT1 and nuclear paraspeckle-mediated mechanism in hepatocellular carcinoma. *Theranostics* **12**, 3518–3533. https://doi.org/10.7150/thno.72581 (2022).
18. Shen, S. et al. CircECE1 activates energy metabolism in osteosarcoma by stabilizing c-Myc. *Mol. Cancer* **19**, 151. https://doi.org/10.1186/s12943-020-01269-4 (2020).
19. Adriaens, C. et al. p53 induces formation of NEAT1 lncRNA-containing paraspeckles that modulate replication stress response and chemosensitivity. *Nat. Med.* **22**, 861–868. https://doi.org/10.1038/nm.4135 (2016).
20. Chakravarty, D. et al. The oestrogen receptor alpha-regulated lncRNA NEAT1 is a critical modulator of prostate cancer. *Nat. Commun.* **5**, 5383. https://doi.org/10.1038/ncomms6383 (2014).
21. Li, R., Harvey, A. R., Hodgetts, S. I. & Fox, A. H. Functional dissection of NEAT1 using genome editing reveals substantial localization of the NEAT1_1 isoform outside paraspeckles. *RNA* **23**, 872–881. https://doi.org/10.1261/rna.059477.116 (2017).
22. Koh, W.-J. et al. Cervical cancer, version 3.2019 NCCN clinical practice guidelines in oncology. *J. Natl. Compr. Cancer Netw.* **17**, 64–84. https://doi.org/10.6004/jnccn.2019.0001 (2019).
23. Statello, L., Guo, C.-J., Chen, L.-L. & Huarte, M. Gene regulation by long non-coding RNAs and its biological functions. *Nat. Rev. Mol. Cell Biol.* **22**, 96–118. https://doi.org/10.1038/s41580-020-00315-9 (2021).
24. Xiang, S. et al. LncRNA IDH1-AS1 links the functions of c-Myc and HIF1α via IDH1 to regulate the Warburg effect. *Proc. Natl. Acad. Sci. U.S.A.* https://doi.org/10.1073/pnas.1711257115 (2018).
25. Li, L., Ma, Y., Maerkeya, K., Reyanguly, D. & Han, L. LncRNA OIP5-AS1 regulates the warburg effect through miR-124-5p/IDH2/HIF-1α pathway in cervical cancer. *Front. Cell Dev. Biol.* **9**, 655018. https://doi.org/10.3389/fcell.2021.655018 (2021).
26. Smith, N. E., Spencer-Merris, P., Fox, A. H., Petersen, J. & Michael, M. Z. The long and the short of it: NEAT1 and cancer cell metabolism. *Cancers* **14**, 4388. https://doi.org/10.3390/cancers14184388 (2022).
27. Park, M. K. et al. NEAT1 is essential for metabolic changes that promote breast cancer growth and metastasis. *Cell Metab.* **33**, 2380-2397.e9. https://doi.org/10.1016/j.cmet.2021.11.011 (2021).
28. Liang, J., Liu, C., Xu, D., Xie, K. & Li, A. LncRNA NEAT1 facilitates glioma progression via stabilizing PGK1. *J. Transl. Med.* **20**, 80. https://doi.org/10.1186/s12967-022-03273-2 (2022).
29 Kartha, R. V. & Subramanian, S. Competing endogenous RNAs (ceRNAs): New entrants to the intricacies of gene regulation. *Front. Genet.* https://doi.org/10.3389/fgene.2014.00008 (2014).
30. Zhou, H. et al. Recent advances of NEAT1-miRNA interactions in cancer. *ABBS* **54**, 153–162. https://doi.org/10.3724/abbs.2021022 (2022).
31. Gao, C., Sun, J., Zhang, Z. & Xu, Z. NEAT1 boosts the development of thoracic aortic aneurysm through targeting miR-324-5p/RAN. *Arch. Med. Res.* **53**, 93–99. https://doi.org/10.1016/j.arcmed.2021.06.009 (2022).
32 Wei, F. et al. LncRNA-NEAT1 inhibits the occurrence and development of pancreatic cancer through spongy miR-146b-5p/traf6. *Biotechnol. Genet. Eng. Rev.* https://doi.org/10.1080/02648725.2023.2192059 (2023).
33. Xu, Y. et al. LINC00943 is correlated with gastric cancer and regulates cancer cell proliferation and chemosensitivity via hsa-miR-101-3p. *Int. J. Clin. Oncol.* **26**, 1650–1660. https://doi.org/10.1007/s10147-021-01945-5 (2021).
34. Cui, G. et al. Glycogen phosphorylase B is regulated by miR101-3p and promotes hepatocellular carcinoma tumorigenesis. *Front. Cell Dev. Biol.* **8**, 566494. https://doi.org/10.3389/fcell.2020.566494 (2020).
35. Hernández-Toledano, D. S. & Vega, L. Methylated dialkylphosphate metabolites of the organophosphate pesticide malathion modify actin cytoskeleton arrangement and cell migration via activation of Rho GTPases Rac1 and Cdc42. *Chem. Biol. Interact.* **382**, 110593. https://doi.org/10.1016/j.cbi.2023.110593 (2023).
36. Ni, J. et al. Tumour-derived exosomal lncRNA-SOX2OT promotes bone metastasis of non-small cell lung cancer by targeting the miRNA-194-5p/RAC1 signalling axis in osteoclasts. *Cell Death Dis.* **12**, 662. https://doi.org/10.1038/s41419-021-03928-w (2021).
37. Wang, C., Yan, G., Zhang, Y., Jia, X. & Bu, P. Long non-coding RNA MEG3 suppresses migration and invasion of thyroid carcinoma by targeting of Rac1. *Neoplasma* **62**, 541–549. https://doi.org/10.4149/neo_2015_065 (2015).

Acknowledgements

We are very grateful for the data provided by the public platform.

Author contributions

Lingling Cao, Wumidan Abudureheman: Conceptualization, Methodology, Software, Investigation, Formal analysis, Writing – original draft. Guqun Shen: Investigation, Resources, Data curation. Yunshan Ouyang , Wang Yang , Qian Zhao, Tianze Lu: Visualization, Investigaion, Supervision. Chen Lin: Conceptualization, Funding acquisition, Resources, Supervision, Writing – review & editing.

Funding

This research was funded by National Natural Science Foundation of China Regional Fund Program, Grant Number 82060473 and 82460557.

Declarations

Competing interests
The authors declare no competing interests.

Informed Consent
All patients gave informed consent for the specimens in this article.

Additional information
Supplementary Information The online version contains supplementary material available at https://doi.org/10.1038/s41598-025-01698-5.

Correspondence and requests for materials should be addressed to C.L.

Reprints and permissions information is available at www.nature.com/reprints.

Publisher's note Springer Nature remains neutral with regard to jurisdictional claims in published maps and institutional affiliations.